energies

MDPI

Article

Research on the Oil Cooling Structure Design Method of Permanent Magnet Synchronous Motors for Electric Vehicles

Shijun Chen [1,2,*], Cheng Miao [1], Xinyu Chen [1], Wei Qian [1] and Songchao Chu [2]

[1] School of Electronic Engineering and Intelligent Manufacturing, Anqing Normal University, Anqing 246133, China; Y23080018@stu.aqnu.edu.cn (C.M.); y22080002@stu.aqnu.edu.cn (X.C.); Y24080034@stu.aqnu.edu.cn (W.Q.)
[2] Anhui Tongfeng Electronics Co., Ltd., Tongling 244000, China; chu.songchao@tong-feng.com
* Correspondence: chenshijun@aqnu.edu.cn

Abstract: Permanent magnet synchronous motors for electric vehicles (EVs) prioritize high power density and lightweight design, leading to elevated thermal flux density. Consequently, cooling methods and heat conduction in stator windings become critical. This paper proposes a compound cooling structure combining direct oil spray cooling on stator windings and housing oil channel cooling (referred to as the winding–housing composite oil cooling system) for permanent synchronous motors in EVs. A systematic design methodology for oil jet nozzles and housing oil channels is investigated, determining the average convective heat transfer coefficient on end-winding surfaces and the heat dissipation factor of the oil channels. Finite element analysis (FEA) was employed to simulate the thermal field of a 48-slot 8-pole oil-cooled motor, with further analysis on the effects of oil temperature and flow rate on motor temperature. Based on these findings, an optimized oil-cooled structure is proposed, demonstrating enhanced thermal management efficiency. The results provide valuable references for the design of cooling systems in oil-cooled motors for EV applications.

Keywords: permanent magnet synchronous motors for electric vehicles (PMSMs-EVs); oil-cooled motors; oil jet nozzles; housing oil channels; oil temperature and flow rate

check for updates

Academic Editor: Adolfo Dannier

Received: 18 May 2025
Revised: 8 June 2025
Accepted: 13 June 2025
Published: 14 June 2025

Citation: Chen, S.; Miao, C.; Chen, X.; Qian, W.; Chu, S. Research on the Oil Cooling Structure Design Method of Permanent Magnet Synchronous Motors for Electric Vehicles. *Energies* **2025**, *18*, 3134. https://doi.org/10.3390/en18123134

Copyright: © 2025 by the authors. Licensee MDPI, Basel, Switzerland. This article is an open access article distributed under the terms and conditions of the Creative Commons Attribution (CC BY) license (https://creativecommons.org/licenses/by/4.0/).

1. Introduction

With the increasingly stringent demands for motor power density in new energy vehicles, traditional air- and water-cooling technologies are approaching their thermal limits. Against this backdrop, oil cooling technology has become a research hotspot due to its high dielectric constant, non-magnetic properties, high insulation, and strong convective heat transfer capabilities. The EU Motor Efficiency Enhancement Plan explicitly states that all motors with output power between 75 and 200 kW must meet IE4 or higher international efficiency standards starting from July 2023. This has directly accelerated the engineering application of oil cooling technology. Reference [1] optimized the thermal performance of an aerospace oil-cooled motor by analyzing its internal oil flow patterns through CFD modeling. Reference [2] designed an oil-cooling-centric thermal management structure to address the performance limitations caused by heat dissipation challenges in hub motors, establishing a thermal distribution model validated by simulations and experiments. Reference [3] investigated the thermal performance of oil-cooled permanent magnet synchronous motors (PMSMs), analyzing their cooling efficiency under different oil parameters.

Oil-cooled motors are primarily categorized into direct and indirect cooling based on the contact form between the cooling oil and the stator yoke. Indirect oil cooling, implemented via housing oil channels [4], enables non-contact heat dissipation with advantages such as good sealing and simplified maintenance. However, excessive thermal resistance layers limit heat transfer efficiency. Direct oil cooling, achieved through immersion or spray methods [5], allows direct contact between the cooling oil and heat-generating components. For example, Reference [6] studied the thermal and economic characteristics of direct oil cooling in electric traction motors, considering variations in cooling oils and drive duty cycles. Notably, the end windings—the largest heat source in motors—directly impact system reliability through their cooling efficiency. Moreover, spray cooling with different flow rates, velocities, nozzle types (e.g., pressure nozzles), and nozzle quantities exhibits distinct effects on winding temperatures and heat transfer coefficients. Reference [7] concluded that full-cone nozzles offer superior heat dissipation efficiency, while hollow-cone nozzles provide better temperature uniformity.

In recent years, hybrid cooling solutions leveraging multi-physics synergy have emerged as breakthrough strategies. For instance, Reference [8] proposed a shaft-housing coupled cooling method that reduces motor temperatures by over 20 °C. Spray + immersion combinations have also been adopted to enhance heat dissipation. However, existing research predominantly focuses on single-component optimization, lacking system-level thermal management design:

(1) The matching mechanism between spray parameters and oil channel structures remains unclear.
(2) The oil pressure balancing challenge in multiple cooling paths leads to local flow stagnation.
(3) The impact of hybrid cooling on electromagnetic performance has not yet been quantified.

Reference [9] highlights efforts to integrate spray cooling technology into EV motors, discussing the advancements and challenges of this novel thermal management approach in enhancing the power density of electric traction motors.

Reference [10] studied an indirectly oil-cooled permanent magnet traction motor with a rated power of 100 kW and a rated speed of 4000 r/min. Heat dissipation is achieved through oil channels designed on the motor housing. Cooling oil at 25 °C removes 5 kW of heat, demonstrating excellent cooling performance. Reference [11] investigated the thermal structure and temperature field of an indirectly oil-cooled switched reluctance starter/generator. The study first calculated motor losses using finite element software and designed an indirect oil-cooling structure characterized by a large heat dissipation area, low internal resistance, and superior sealing. Cooling oil extracts heat via convective heat transfer within an axial helical structure.

Direct oil-cooled motors differ from indirect ones in cooling structure and heat transfer processes. Direct cooling involves oil directly contacting heat sources (e.g., windings) to remove heat through convection. This method suits motors operating under high thermal loads and harsh environments. However, the complex internal oil flow patterns in direct cooling systems make accurate temperature field calculations challenging, necessitating advanced modeling for theoretical and practical guidance. Reference [12] explored a direct oil-cooling system for EV motors, combining spray cooling and circulatory oil cooling. Oil indirectly extracts heat via housing channels while being directly sprayed onto windings and stator/rotor ends, significantly enhancing cooling for end windings and permanent magnets.

Reference [13] improved the cooling and lubrication of a direct oil-cooled motor by designing oil channels within the hollow shaft to cool winding ends, bearings, and gears. Orthogonal matrix analysis optimized key cooling parameters, resulting in a system outperforming traditional designs. Reference [14] describes Tesla's compound hollow shaft

sleeve with dual annular chambers. Oil flows inward, reverses direction at a sealed wall, and exits through an outer chamber in contact with the rotor, providing supplemental cooling. Reference [15] details Tesla's hybrid system combining shaft and housing cooling: oil first cools the rotor via centrifugal pumping, then flows to the housing for stator cooling and ambient heat exchange.

Reference [16] implemented in-slot oil cooling by designing axial oil channels adjacent to stator windings. Heat transfers from windings to channels via slot contacts, but increased airgap length (to prevent oil leakage into the rotor) reduces magnetic loading and raises thermal stress. Slot cooling also lowers the slot fill ratio, reducing efficiency. Despite superior cooling, its high cost and design complexity limit applications to niche markets. Reference [17] utilized spray ring cooling, where automatic transmission fluid (ATF) is sprayed onto winding ends via nozzles, achieving uniform cooling across internal and external surfaces. Reference [18] positioned spray nozzles near stator windings, relying on gravity for oil distribution. While spray cooling offers 2.5–5× higher heat removal than air cooling, uneven oil distribution due to gravity and rotor rotation creates temperature gradients, necessitating hybrid approaches (e.g., spray + housing or spray + immersion).

Conclusion: Balancing structural feasibility, manufacturability, cost, and cooling efficiency, this study adopts a combined cooling scheme of direct stator winding spray + housing oil channels. As shown in Figure 1, cooling oil enters through the inlet, sprays onto stator end windings via dual nozzles, flows through housing channels to cool the stator core, and collects in the bottom reservoir before exiting through the outlet. This structure ensures sufficient cooling for the stator windings while simultaneously enabling stator core cooling through the cooling oil. By designing appropriate oil reservoirs and strategically positioned oil outlets, the stator core can be fully immersed in the cooling oil, thereby achieving enhanced cooling performance.

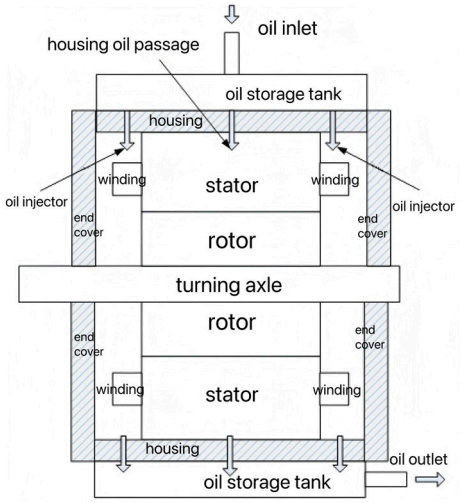


Figure 1. Combined cooling structure of direct spray on stator windings and housing oil channels.

2. Oil Cooling Structure Design for PMSMs-EVs

2.1. Design of Oil Jet Nozzles

The prototype stator windings adopt direct spray cooling, with two oil jet nozzles positioned above each end of the stator windings. The nozzle orifice size and placement directly determine the oil film thickness on the end windings, critically influencing their cooling effectiveness. Given the complexity of the end-winding oil spray paths, finite element analysis (FEA) and multivariate nonlinear fitting theory were employed to comprehensively analyze the impact of nozzle orifice size and positioning on the thermal dissipation performance of the motor's end windings.

Assuming all heat losses from the end windings are removed by the cooling oil, Newton's law of cooling gives the following:

$$P_{cu_end} = hA_{endw}(T_{max} - T_f), \tag{1}$$

where P_{cu_end} is the copper loss of the end windings; h and A_{endw} are the convective heat transfer coefficient and convective heat transfer area of the end windings, respectively; T_{max} and T_f are the maximum temperature on the end windings and the cooling oil temperature, respectively.

From Equation (1), the maximum temperature estimation formula for the motor's end windings can be derived as follows:

$$T_{max} = \frac{P_{cu_end}}{hA_{endw}} + T_f = \frac{P_{cu_end}}{\gamma_{end}} + T_f, \tag{2}$$

where γ_{end} is the heat dissipation factor of the end windings, defined as $\gamma_{end} = hA_{endw}$.

As indicated by Equation (2), under constant end-winding losses, the maximum temperature rise of the motor's end windings depends on the heat dissipation factor γ_{end}. A higher γ_{end} signifies superior cooling performance, while a lower value indicates inferior thermal management.

Figure 2 shows the simulation model of the oil jet nozzle and end windings, where the nozzle diameter is denoted as D_w, and the height of the end windings is H_w. The simulation parameters include an inlet oil temperature of 90 °C, an inlet flow rate of 5 L/min (automatic transmission fluid, thermal conductivity: 0.2 W/m·°C, specific heat capacity: 1963 J/(kg·°C), density: 846 kg/m^3, dynamic viscosity: 0.0066 Pa·s), and copper losses of 474.7 W per end winding. A 3D finite element simulation was conducted to analyze the influence of nozzle diameter D_w and end-winding height H_w on the average convective heat transfer coefficient ($h_{average}$) of the end-winding surfaces. Since the surface area of the end windings is fixed, a higher $h_{average}$ directly increases the heat dissipation factor (γ_{end}), thereby improving cooling performance.

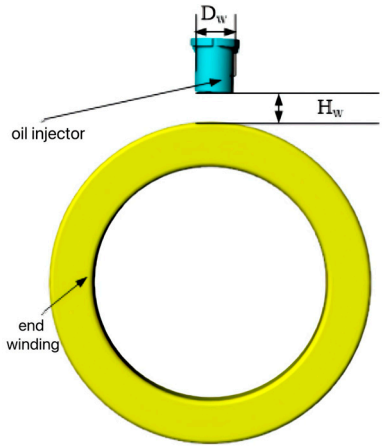
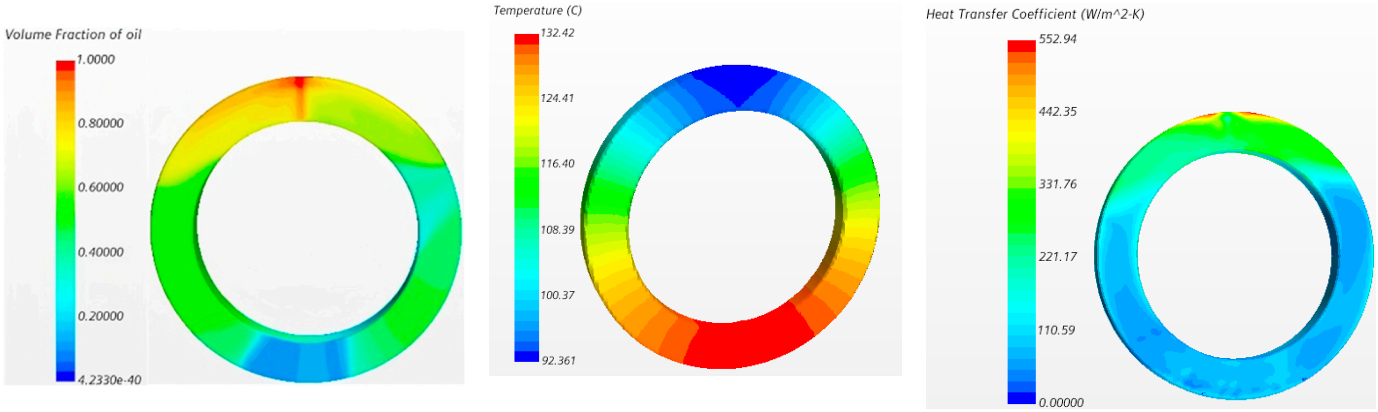


Figure 2. Simulation model of the oil jet nozzle and end windings.

Figure 3 shows the temperature rise simulation results of the end windings with an oil jet nozzle orifice diameter of 1 mm and a vertical position height of 16 mm. In the simulation: value = 1 indicates the corresponding region is fully occupied by cooling oil; value = 0 indicates the region is entirely filled with air. The results reveal that directly below the nozzle, the end windings exhibit the highest concentration of cooling oil, leading to the maximum convective heat transfer coefficient and the lowest temperature of 92.4 °C.

Under gravity, the cooling oil flows along the end surfaces of the windings. However, at the bottommost section of the end windings, the oil coverage diminishes significantly, resulting in the highest localized temperature of 132.4 °C.



(**a**) (**b**) (**c**)

Figure 3. Thermal field simulation analysis of end windings. (**a**) Cooling oil volume fraction distribution; (**b**) temperature distribution; (**c**) surface convective heat transfer coefficient distribution.

Using the same analytical method, by varying two parameters—the nozzle orifice diameter and vertical position height—we obtained 49 distinct configurations of the average convective heat transfer coefficient ($h_{average}$ (W/m^2/K)) for the end-winding surfaces, as detailed in Table 1.

Table 1. Average convective heat transfer coefficient of end-winding surfaces (unit: W/m^2/K).

D_w (mm) \ H_w (mm)	3	6	9	12	16	20	30
1	154.1	151.7	148.8	153.3	166.1	164	156.9
2	129.1	123.8	139.1	126.2	125	129.4	122.7
5	109	103	98.7	87.8	90.5	104.4	88.2
10	90.7	86.9	76	75.28	85.3	87.2	76.1
15	79.6	77.2	70.1	52.9	58.1	75.2	54.7
20	74.1	66.4	62.2	45.3	55.7	48.4	49.6
30	66.4	53.4	49.6	45.7	40.3	37.8	46.6

Using multivariate nonlinear regression theory, the simulation data from Table 1 were fitted to derive the nonlinear relationship between the convective heat transfer coefficient ($h_{average}$) and the nozzle diameter (D_w) and vertical position height (H_w). The analytical procedure is as follows [19]:

Establish the regression function

$$\hat{Y} = f(X_i, b_i, b_0), \tag{3}$$

where $\hat{Y}$ is the estimated value of the dependent variable Y; X_i are the independent variables; b_0 and b_i represent the constant term and regression coefficients, respectively.

Residual calculation

$$e_k = y_k - \hat{y}_k (k = 1, 2, 3 \ldots\ldots n), \tag{4}$$

where y_k and $\hat{y}_k$ represent the observed value and calculated value of the dependent variable, respectively; e_k denotes the deviation between the observed and calculated values; k indicates the observation index.

The objective function of regression analysis:

$$\sum_{k=1}^{n} e_k^2 = \sum_{k=1}^{n} (y_k - \hat{y}_k)^2 \rightarrow \min, \tag{5}$$

Based on Equations (3)–(5) and the data from Table 1, the expression for the average convective heat transfer coefficient ($h_{average}$) of the end-winding surfaces was derived through regression fitting.

$$\begin{aligned} h_{average} = {} & 168.6 - 12.6D_w - 3.253H_w + 0.6896D_w^2 - 0.2149H_wD_w + 0.2858H_w^2 \\ & - 0.01196D_w^3 + 0.00204D_w^2H_w + 0.003833\ D_wH_w^2 - 0.006227H_w^3 \end{aligned}, \tag{6}$$

This formula serves as a critical design basis for selecting the nozzle diameter and vertical positioning height in stator end-winding spray cooling systems, enabling rapid optimization of oil-jet nozzle configurations.

As calculated from Equation (6), Figure 4 illustrates the relationship between the average convective heat transfer coefficient $h_{average}$ of the end-winding surfaces and the nozzle diameter D_w and positioning height H_w. The results demonstrate that $h_{average}$ decreases with increasing nozzle diameter, while the positioning height exhibits a nonlinear correlation with the heat transfer coefficient. Design optimization requires a comprehensive consideration of factors including pump power, spatial constraints, cost, and manufacturing feasibility.

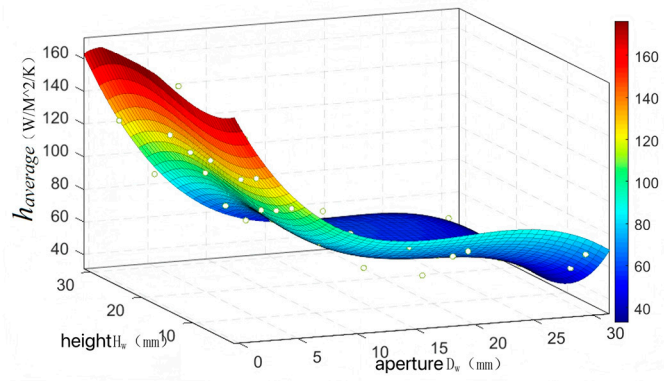


Figure 4. Surface plot of the average convective heat transfer coefficient $h_{average}$ on end-winding surfaces as a function of D_w and H_w.

Based on Equation (6), the heat dissipation factor of the end windings is obtained as follows:

$$\gamma_{end} = h_{average}A_{endw} = \frac{\pi h_{average}}{4}(D_{ts}^2 - D_{is}^2) + l_{endw}\pi h_{average}(D_{ts} + D_{is}), \tag{7}$$

where l_{endw} is the length of the end windings, D_{ts} and D_{is} denote the tooth root diameter and stator inner diameter of the motor, respectively.

2.2. Design of Housing Oil Channels

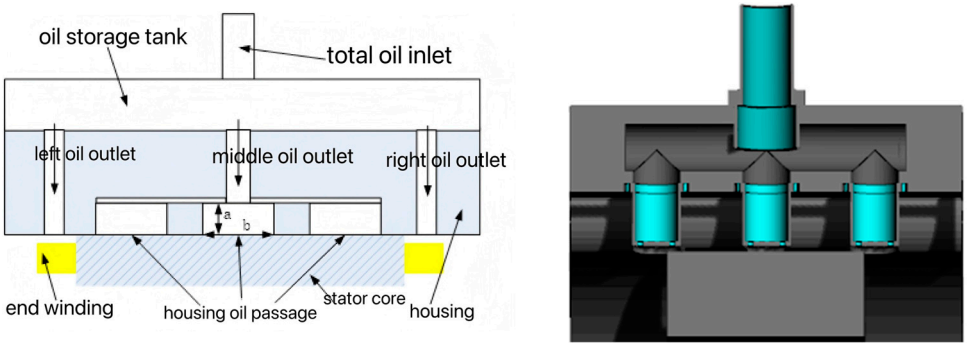
Given the manufacturing challenges and poor feasibility of axial helical oil grooves on the inner wall of the motor housing, as well as the adverse impact of stator yoke oil channels on the magnetic circuit, this chapter adopts a circular groove structure on the housing inner wall. The width and depth of the housing oil channels critically determine the thermal

dissipation performance of the stator core, while also requiring careful consideration of the housing's mechanical structural strength.

As illustrated in Figure 5, each oil channel operates independently. Cooling oil flows from the main inlet into the top oil reservoir, then distributes through intermediate ports to the housing oil channels, and finally collects in the bottom oil reservoir. Within the channels, the oil flow exhibits three distinct regimes, and the convective heat transfer coefficient under each regime is determined by the Nusselt number (N_u), calculated as follows [20]:

$$N_u = \begin{cases} 3.66, R_e \leq 2200.0 \\ 0.012(R_e^{0.87} - 280)P_r^{0.4}[1 + (d/l)^{2/3}](\frac{p_{rf}}{p_{rw}})^{0.11}, 2200.0 < R_e < 10^4 \\ 0.023R_e^{0.8}P_r^{0.4}, R_e \geq 10^4 \end{cases}, \quad (8)$$

where R_e and P_r are the Reynolds number and Prandtl number, respectively; d and l represent the hydraulic diameter and length of the housing oil channels, respectively; P_{rf} and P_{rw} represent the Prandtl numbers calculated with the fluid temperature and the wall temperature as the characteristic temperatures, respectively.



(**a**) (**b**)

Figure 5. Schematic of the motor housing oil channels. (**a**) Planar schematic; (**b**) three-dimensional structure.

Under specified flow rate and pressure design requirements, the head loss within the housing oil channels directly impacts their cooling effectiveness. Since each housing oil channel has no joints or bends, the cooling oil flow experiences only frictional head loss (also termed major head loss) along the straight channel segments. This loss is proportional to the channel length l and inversely proportional to the hydraulic diameter d. The head loss can be calculated using the following formula:

$$H_f = \xi \frac{l}{d} \frac{V_{oil}^2}{2g}, \quad (9)$$

In the equation, ξ represents the frictional head loss coefficient, V_{oil} is the velocity of the cooling oil within the channel, and g denotes the gravitational acceleration.

Assuming all heat generated by the stator core and slot windings is dissipated by the cooling oil in the housing oil channels, the heat dissipation factor of the housing oil channels (γ_f) can be derived using the same computational method as Equation (2). A higher γ_f indicates a stronger cooling capacity of the oil channels. By optimizing the cross-sectional dimensions of the channels, γ_f can be maximized. Additionally, the motor housing must satisfy mechanical structural strength requirements.

Within the housing oil channels, the cooling oil flow velocity (V), hydraulic diameter (d), convective heat transfer coefficient (h_{fo}), and heat transfer area of the oil channels (A_{fo}) can be calculated using Equation (10):

$$\begin{cases} V = \frac{Q_i}{N_f ab} \\ d = \frac{2ab}{a+b} \\ R_e = \frac{\rho V d}{\mu_f} \\ h_{fo} = \frac{\lambda_{oil} N_u}{d} \\ A_{fo} = (a+b) N_f \pi D_{os} \end{cases}, \tag{10}$$

In the equation, Q_i is the total inlet oil flow rate; μ_f and λ_{oil} are the dynamic viscosity of the fluid and the thermal conductivity of the cooling oil, respectively; a and b are the depth and width dimensions of the housing oil channels, respectively; D_{os} is the outer diameter of the motor stator; N_f is the number of oil channels in the housing.

Combining Equations (8) and (10), the formula for calculating the heat dissipation factor (γ_f) of the housing oil channels is derived as follows:

$$\gamma_f = h_{fo} A_{fo} = \begin{cases} \frac{3.66 \lambda_{oil} (a+b)^2 N_f \pi D_{os}}{2ab}, R_e \leq 2200.0 \\ \frac{0.012 \lambda_{oil} (a+b)^2 N_f \pi D_{os}}{2ab} (R_e^{0.87} - 280) P_r^{0.4} [1 + (\frac{4ab}{(a+b)\pi D_{os}})^{2/3}] (\frac{p_{rf}}{p_{rw}})^{0.11}, 2200.0 < R_e < 10^4 \\ \frac{0.023 \lambda_{oil} (a+b)^2 N_f \pi D_{os}}{2ab} R_e^{0.8} P_r^{0.4}, R_e \geq 10^4 \end{cases}, \tag{11}$$

Based on the above, the design methodology for the housing oil channel of PMSMs-EVs can be summarized as follows: Under specified flow rate and pressure requirements, calculate the cooling oil velocity within the housing oil channel, the hydraulic diameter of the channel, and the Reynolds number using Formula (10). Combined with Formulas (8) and (10), determine the flow regime based on the Reynolds number, then compute the corresponding average Nusselt number and convective heat transfer coefficient. Subsequently, calculate the housing heat dissipation factor using Formula (11)—a higher heat dissipation factor indicates better cooling performance. Finally, validate the mechanical structural strength of the motor housing using finite element software to select the optimal dimensional parameters for the housing oil channel.

3. Thermal Field Simulation Analysis of the Electric Motor

3.1. Dimensional Parameters of the Prototype

The prototype analyzed in this study is 48-slot 8-pole PMSMs-EVs. Its technical specifications and primary parameters are summarized in Tables 2 and 3, respectively.

Table 2. Technical specifications and key dimensional requirements of the prototype.

Parameter	Value	Parameter	Value
Rated Power (kW)	50	Maximum Torque (N·m)	120
Rated Speed (r/min)	4775	DC Bus Voltage (V)	350
Rated Torque (N·m)	100	Maximum Current (RMS, A)	210
Maximum Power (kW)	70	Maximum Core Length (mm)	90
Maximum Speed (r/min)	7000	Maximum Stator Core Outer Diameter (mm)	210
Peak Motor Operating Efficiency	≥94%	Winding Temperature (°C)	≤155
Proportion of Efficiency ≥ 85% Region	≥85%	Peak Motor System Efficiency	≥91%

Table 3. Primary Parameters of the Prototype.

Parameter	Value	Parameter	Value
Stator Outer Diameter (mm)	210	Rotor Inner Diameter (mm)	67
Core Axial Length (mm)	90	Poles/Slots	8/48
Silicon Steel Material	B27AHV1400	Magnet Material	N48UH
Cooling Method	Oil Cooling		

The prototype employs a combined oil cooling structure featuring direct oil spray on end windings and housing oil channels. The cooling oil inlet flow rate is set to 5 L/min, with an inlet static temperature of 90 °C. Based on Equation (6), the nozzle orifice diameter and positioning height were designed to achieve the maximum average convective heat transfer coefficient on the end-winding surfaces. Substituting relevant parameters into Equations (8)–(10), the calculated Reynolds number (R_e), heat dissipation factor (γ_f) of the housing oil channels, and pressure drop (P) between the inlet and outlet are as follows:

$$R_e = \frac{2\rho Q_i}{N_f(a+b)u} = \frac{21.4}{N_f(a+b)}, \tag{12}$$

$$\gamma_f = \frac{0.066N_f(a+b)^2}{ab} \times N_u, \tag{13}$$

$$P = \xi\frac{4.84(a+b) \times 10^{-7}}{a^3b^3}, \tag{14}$$

3.2. Prototype Thermal Field Simulation and Result Analysis

Using Equations (8), (12) and (13), the relationship between the heat dissipation factor (γ_f) and the parameters N_f, a, and b is established, while satisfying the requirement of Equation (14) (pressure drop between oil channel inlet and outlet $\leq$ 15 kPa). The mechanical structural strength of the motor housing is then verified via finite element analysis (FEA). The key dimensional parameters of the designed prototype oil cooling structure are listed in Table 4.

Table 4. Key dimensional parameters of the prototype oil cooling structure.

Parameter	Value
Nozzle Diameter (mm)	1
Nozzle Height (mm)	16
Number of Housing Oil Channels	2
Housing Oil Channel Depth (mm)	2
Housing Oil Channel Width (mm)	19

To facilitate polyhedral meshing and reduce computational workload, components within the motor were appropriately simplified without compromising the accuracy of temperature distribution. Figure 6 illustrates the simplified 3D model of the motor used for simulation.

Table 5 specifies the material properties of motor components. Table 6 provides the loss distribution values under continuous operation at both rated speed (4775 r/min) and maximum speed (7000 r/min).

The simplified 3D motor model was imported into finite element software to simulate the three-dimensional temperature field distribution under two operating conditions: 4775 r/min @ 100 Nm and 7000 r/min @ 68.2 Nm. For the 4775 r/min @ 100 Nm condition, the cooling oil volume fraction distribution inside the motor is shown in Figure 7, where a

value of 1 indicates full oil occupancy, 0 represents pure air, and the distribution reflects the internal oil flow paths. The results reveal a mixed oil–air distribution within the motor. Oil jet nozzles directly spray cooling oil onto both end windings, and under gravity, the oil flows along the end-winding surfaces to the bottom. Simultaneously, cooling oil on the outer surface of the stator core flows through housing oil channels to the motor base, where it collects in the bottom reservoir. However, the oil volume is insufficient to fully submerge the stator core.

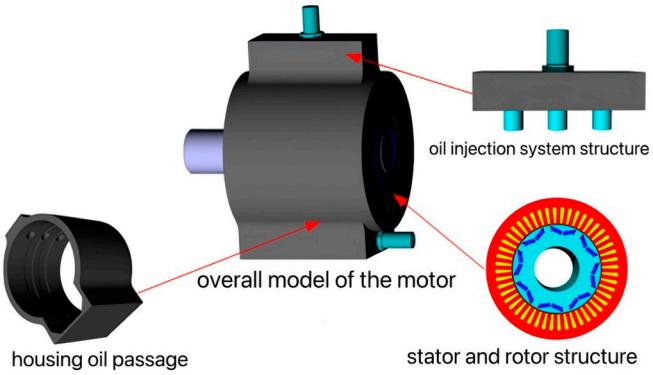


Figure 6. 3D Simplified model of the prototype.

Table 5. Material properties of motor components.

Motor Component	Thermal Conductivity [W/m·°C]	Specific Heat Capacity [J/(kg·°C)]	Density [kg/m^3]	Dynamic Viscosity [Pa·S]
Housing	168	833	2790	-
End Cover	168	833	2790	-
Shaft	52	460	7800	-
Core	30	460	7650	-
Copper Wire	401	385	8933	-
Magnet	7.6	460	7500	-
Air	0.0242	1007	1.225	-
Insulating Varnish	0.15	930	800	-
Slot Insulation	0.19	1300	800	-
Cooling Oil	0.2	1963	846	0.0066

Table 6. Power loss values at rated and maximum continuous speeds.

Loss Type \ Operating Condition	4775 r/min@100 N·m	7000 r/min@68.2 N·m
Copper Loss (W)	1898.7	1091.1
Core Iron Loss (W)	1170.6	1571.1
Permanent Magnet Eddy Current Loss (W)	20	35
Mechanical Loss (W)	127.3	186.6

Figure 8 shows the temperature contour map of motor components under the 4775 r/min @ 100 Nm condition. The highest temperature on the outer surface of the stator core is located at the motor base. Notably, the maximum winding temperature no longer occurs at the end windings but instead appears in the slot windings at the base. This phenomenon arises because cooling oil flowing through the housing oil channels toward the motor base diminishes in quantity, and the collected oil in the bottom reservoir is insufficient to submerge the stator core.

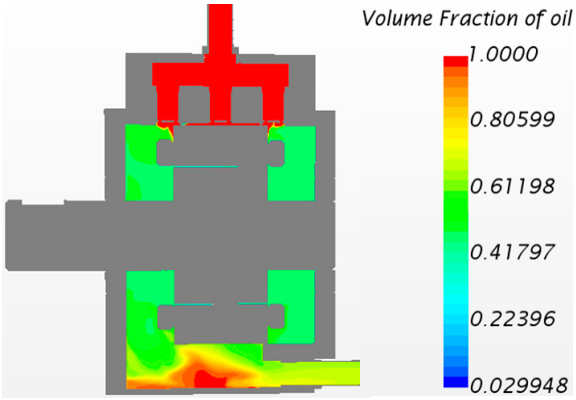


Figure 7. Cooling oil volume fraction distribution inside the motor at 4775 r/min@100 Nm.

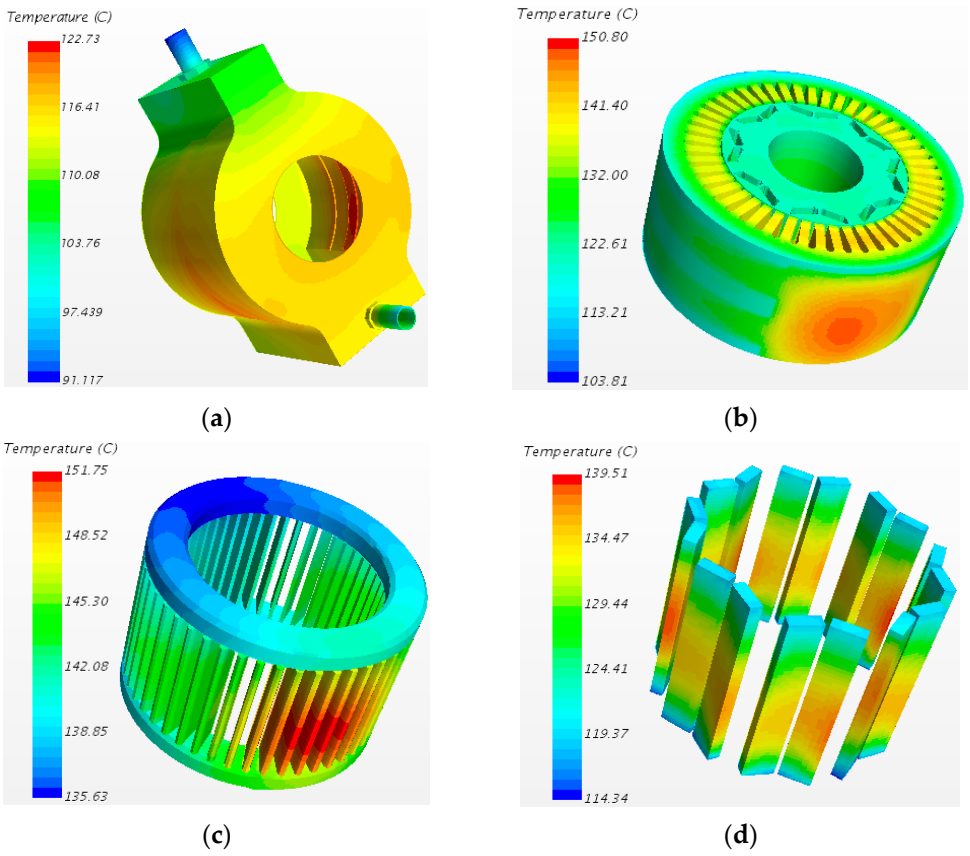


Figure 8. Temperature contour maps of motor components at 4775 r/min@100 Nm: (**a**) temperature distribution of oil channel inlet/outlet and housing; (**b**) temperature distribution of stator and rotor cores; (**c**) Temperature distribution of stator windings; (**d**) temperature distribution of permanent magnets.

As shown in Table 7, the highest temperature of the motor does not occur at the end windings but rather at the stator slot windings (4775 rpm @ 100 N·m) or the stator core (7000 rpm @ 68.2 N·m). The overall temperature at 4775 rpm is consistently higher than that at 7000 rpm. This is attributed to the former's total losses being 332.8 W greater than the latter, with copper losses alone increasing by 807.6 W, leading to elevated temperatures.

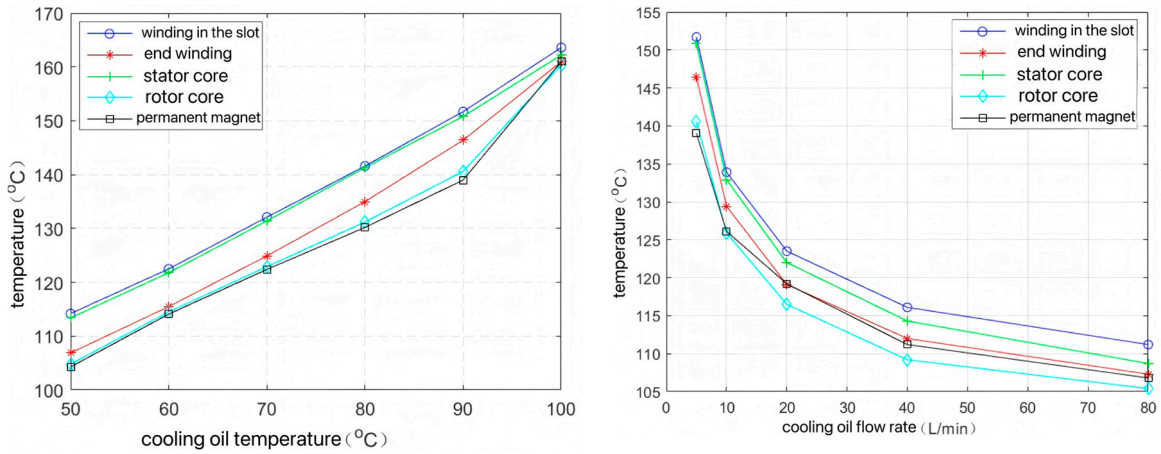
Table 7. Maximum temperature distribution of key motor components.

Operating Condition	Motor Component	Simulated Temperature (°C)
4775 r/min@100 N·m	Oil Inlet Temperature	90.0
	Oil Outlet Temperature	110.6
	Stator Slot Winding	151.8
	End Winding	146.4
	Stator Core	150.8
	Rotor Core	140.6
	Permanent Magnet	139.5
7000 r/min@68.2 N·m	Oil Inlet Temperature	90.0
	Oil Outlet Temperature	106.3
	Stator Slot Winding	138.0
	End Winding	131.1
	Stator Core	142.8
	Rotor Core	138.2
	Permanent Magnet	137.8

4. Analysis of Cooling Oil Temperature and Flow Rate Effects on Thermal Field

Figure 9 shows the simulated temperature variation curves of the motor with oil temperature and flow rate under the 4775 r/min @ 100 Nm operating condition, while maintaining fixed nozzle and housing oil channel dimensions (inlet oil flow rate: 5 L/min). The simulation results reveal the following:

- The temperatures of key motor components increase with rising inlet oil temperature, and the rate of temperature rise accelerates at higher oil temperatures.
- Due to direct oil spray on the end windings and rotor end surfaces, the maximum temperature of stator windings shifts from the end windings to the slot windings, while the rotor and permanent magnets exhibit relatively low-temperature rises. This thermal behavior differs from water-cooled housing designs.
- The critical component temperatures of the prototype decrease with increasing inlet oil flow rate. Below 40 L/min, temperature shows strong flow-rate dependence, though this sensitivity progressively diminishes with higher flow rates. Beyond 40 L/min, further increases in cooling oil flow yield no significant temperature reduction.



(**a**) (**b**)

Figure 9. Variation curves of prototype components with inlet oil temperature and flow rate; (**a**) cooling oil temperature variation; (**b**) cooling oil flow rate variation.

Analysis indicates that when the inlet oil flow rate reaches 15 L/min, the cooling oil completely fills the motor interior, as demonstrated by the volume fraction distribution in Figure 10. This operating condition is not recommended in practice because a fully oil-immersed motor substantially increases rotor damping. The resulting effects include significantly reduced operational efficiency and potential mechanical instability risks.

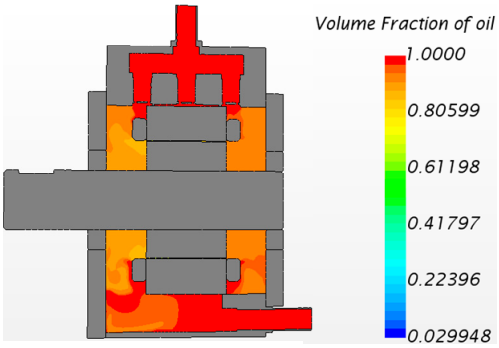


Figure 10. Cooling oil volume fraction distribution at an inlet flow rate of 15 L/min for the prototype.

In summary, while increasing the cooling oil flow rate enhances the motor's cooling effectiveness, it also raises rotor damping and oil pump power consumption, thereby reducing motor efficiency. Consequently, the design must holistically balance cooling performance, motor efficiency, rotor dynamics, and cost to optimally select the cooling oil flow rate. The housing design incorporates only two oil channels, whose relative dimensions are sufficiently small compared to the overall housing size to inherently meet mechanical strength requirements. Therefore, the mechanical stress analysis of the housing was deemed unnecessary and consequently omitted.

5. Improved Design Analysis of the Prototype Oil Cooling Circuit

Analysis of the prototype's temperature distribution reveals excessive temperatures at the stator windings and the base of the stator core. This issue arises because cooling oil flowing toward the end windings and stator core does not accumulate at the base but instead drains directly into the oil reservoir under gravity. The bottom reservoir collects only a small portion of the oil, with most exiting through the oil outlet. To address this limitation and enhance cooling at the base of the stator core and windings, the oil cooling structure was modified by raising the oil outlet position to align with the central height of the bottom-end windings. This adjustment allows the reservoir to retain more cooling oil, thereby improving thermal management for the base regions.

The oil cooling structure of the PMSMs-EVs was redesigned using the finite element simulation method by elevating the position of the oil outlet. The cooling oil volume fraction distribution contour map inside the improved prototype under the 4775 r/min @ 100 Nm operating condition is shown in Figure 11. It can be observed that the amount of cooling oil collected in the motor's bottom reservoir has increased compared to the original model. However, the oil volume at the base remains insufficient to fully submerge the stator core and windings at the motor's bottom.

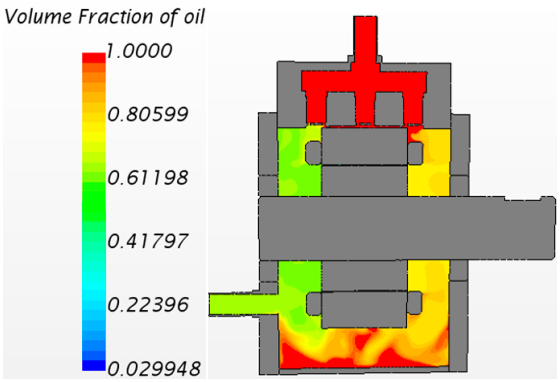


Figure 11. Cooling oil volume fraction distribution contour map inside the improved model at 4775 r/min @ 100 Nm.

Figure 12 shows the temperature distribution contour map of motor components for the improved model under the 4775 r/min @ 100 Nm operating condition. A comparison of temperature rise simulation data between the improved and original models is provided in Table 8. The results indicate that, under identical operating conditions and boundary constraints, the improved motor model exhibits significantly lower temperatures across all critical components compared to the original design, with the highest temperature observed at the stator slot windings (137.0 °C). This improvement stems from relocating the oil outlet upward, which increases oil accumulation in the bottom reservoir and enhances cooling efficiency for the stator core, thereby reducing overall temperatures.

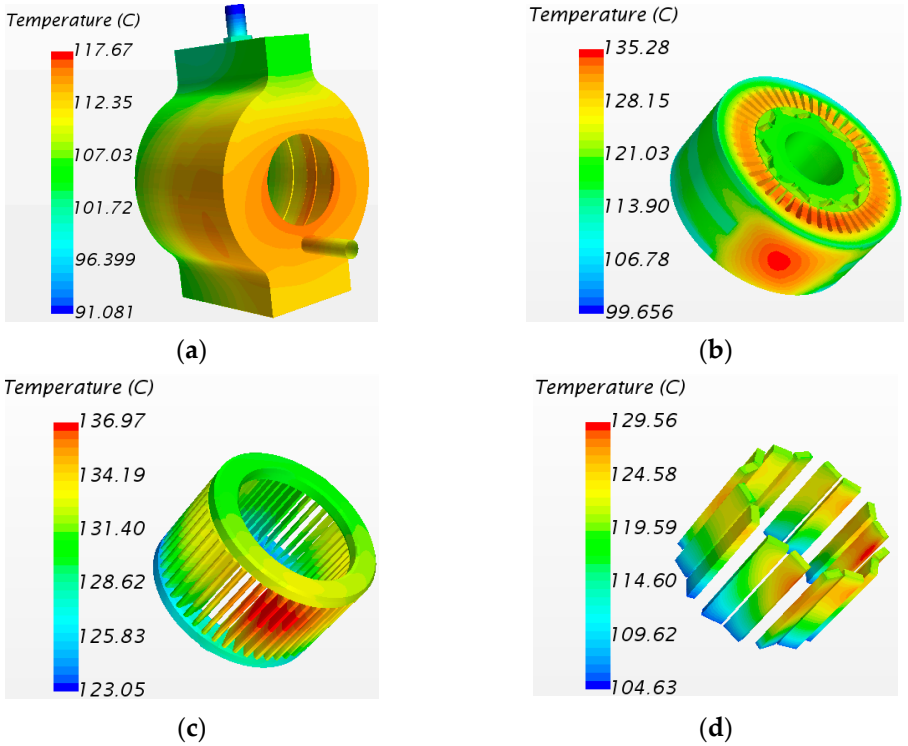


Figure 12. Temperature distribution contour maps of components in the improved prototype at 4775 r/min @ 100 Nm: (**a**) oil channel inlet/outlet and housing; (**b**) stator and rotor cores; (**c**) stator windings; (**d**) permanent magnets.

Table 8. Comparison of temperature simulation results before and after oil cooling structure improvement.

Operating Condition	Motor Component	Temperature (°C) (Original Model)	Temperature (°C) (Improved Model)	Temperature Change Rate ($\frac{T_0-T_1}{T_0}\times 100\%$)
4775 r/min@100 N·m	Oil Inlet	90.0	90.0	0
	Oil Outlet	110.6	116.3	−5.15%
	Stator Slot Winding	151.8	137.0	9.75%
	End Winding	146.4	133.7	8.67%
	Stator Core	150.8	135.3	10.28%
	Rotor Core	140.6	130.2	7.4%
	Permanent Magnet	139.5	129.6	7.1%

Note: T_0 denotes the temperature of the original model, and T_1 represents the temperature of the improved model.

6. Conclusions

The design of cooling and thermal management systems is a critical aspect of high-density, high-efficiency PMSMs-EVs. This study focuses on a winding–housing composite oil-cooling structure, with emphasis on the design methodologies for oil jet nozzles and housing oil channels. Leveraging extensive finite element simulation results and applying multivariate nonlinear regression fitting theory, the average convective heat transfer coefficient ($h_{average}$) on end-winding surfaces was modeled as a bivariate polynomial function of nozzle orifice diameter and positioning height, revealing their intrinsic relationship. The average convective heat transfer coefficient on the end-winding surface decreases with increasing nozzle orifice diameter, while exhibiting a nonlinear relationship with positional height. Equation (6) provides a basis for rapid optimization of nozzle design parameters. For motors of different sizes, the end-winding cooling factor can be efficiently calculated using Equation (7). Furthermore, we have derived the relationship between the housing oil channel's cooling factor and its geometric parameters including channel width, depth, and number of channels. Equation (11) enables quick estimation of the housing oil channel cooling factor for variously sized motors. These formulations collectively establish a theoretical framework for rapid thermal assessment of motor cooling structures.

Using a 48-slot 8-pole oil-cooled motor (rated power: 50 kW) as a case study, the temperature distributions under both rated load/rated speed (4775 r/min @ 100 Nm) and maximum speed (7000 r/min @ 68.2 Nm) conditions were analyzed. The influence of oil temperature and flow rate on thermal performance was systematically investigated. An improved oil-cooling structure was proposed, achieving temperature reductions of 10.28% and 9.75% for the stator core and slot windings, respectively, under rated conditions.

The design methodology presented in this study significantly reduces the development costs for oil channel design and optimization while providing a valuable reference for analogous oil-cooled motor architectures. Key contributions include the following:

- Empirical correlations for $h_{average}$ and γ_f, enabling rapid design iteration.
- Demonstrated thermal performance enhancements via FEA and parametric studies.
- Framework applicable to motors across power ranges and cooling configurations.

Author Contributions: Conceptualization, S.C. (Shijun Chen) and C.M.; methodology, S.C. (Shijun Chen) and C.M.; software, S.C. (Shijun Chen) and C.M.; validation, S.C. (Shijun Chen), C.M., X.C., W.Q. and S.C. (Songchao Chu); formal analysis, S.C. (Shijun Chen); investigation, X.C.; resources, S.C. (Songchao Chu); data curation, W.Q.; writing—original draft preparation, S.C. (Shijun Chen), C.M., X.C., W.Q. and S.C. (Songchao Chu); writing—review and editing, S.C. (Shijun Chen) and C.M. All authors have read and agreed to the published version of the manuscript.

Funding: This research was funded by the Anhui Province Key R&D Program High Tech Field Project, grant number 202304a05020084, and 2024 Anhui Province University Science and Engineering Teachers' Internship Program in Enterprises, grant number. 2024jsqygz47, and the Anhui Province Higher Education Scientific Research Project, grant number 2024AH051084, and the National and Local Joint Engineering Laboratory for High-Efficiency Motors and Control Technologies 2024 Open Fund Project, grant number KFKT202401.

Data Availability Statement: The nature of the data is the motor size parameters; the data can be accessed from the Electrical Machinery Laboratory of Anqing Normal University. The complete data belong to the joint ownership of the Electrical Machinery Laboratory of Anqing Normal University and the enterprise.

Acknowledgments: We would like to thank Anqing Normal University for their support, as well as all the experts and members who provided technical assistance.

Conflicts of Interest: Authors Shijun Chen and Songchao Chu were employed by the company Anhui Tongfeng Electronics Co., Ltd. The remaining authors declare that the research was conducted in the absence of any commercial or financial relationships that could be construed as a potential conflict of interest.

References

1. Li, M.; Yan, B.; Zhou, Y.; Tian, L. Research and Simulation of Flow Field on Aviation Oil-Cooled Motor. *Small Spec. Electr. Mach.* **2022**, *50*, 31–34.
2. Guo, F.; Zhang, C. Oil Cooling Method for Internal Heat Sources in the Outer Rotor Hub Motor of Electric Vehicle and Thermal Characteristics Research. *Energies* **2024**, *17*, 6312. [CrossRef]
3. Yang, C.; Cai, W.; Xie, Y.; Shao, B. Experiment and Simulation Study on the Cooling Performance of Oil-Cooling PMSM with Hairpin Winding. *Machines* **2024**, *12*, 119. [CrossRef]
4. Yu, S.; Zhou, Y.; Wang, Y.; Zhang, J.; Dong, Q.; Tian, J.; Chen, J.; Leng, F. Optimization Study of Cooling Channel for the Oil Cooling Air Gap Armature in a High-Temperature Superconducting Motor. *Electronics* **2023**, *13*, 97. [CrossRef]
5. Gundabattini, E.; Mystkowski, A.; Idzkowski, A.; Singh, R.R.; Solomon, D.G. Thermal mapping of a high-speed electric motor used for traction applications and analysis of various cooling methods—A review. *Energies* **2021**, *14*, 1472. [CrossRef]
6. Garud, K.S.; Lee, M.Y. Heat transfer and economic characteristics of direct oil cooling for electric traction motor under driving cycles. *Appl. Therm. Eng.* **2025**, *258*, 124608. [CrossRef]
7. Liu, C.; Xu, Z.; Gerada, D.; Li, J.; Gerada, C.; Chong, Y.; Popescu, M.; Goss, J.; Staton, D.; Zhang, H. Experimental investigation on oil spray cooling with hairpin winding. *IEEE Trans. Ind. Electron.* **2019**, *67*, 7343–7353. [CrossRef]
8. Zhang, Z.; Song, Q.; Ahmed, B.; Han, Y. Fluid and thermal effect on temperature-dependent power increase of electric vehicle's permanent magnet synchronous motor using compound water cooling method. *Case Stud. Therm. Eng.* **2025**, *65*, 105543. [CrossRef]
9. Kalajahi, A.K.; Ghahfarokhi, P.S. High-Viscosity Spray Cooling System for High-Reliability Motor Drives in Electric Vehicles: A Review. *IEEE Trans. Transp. Electrific.* **2024**, *11*, 3418–3432. [CrossRef]
10. Laskaris, K.I.; Kladas, A.G. Liquid Cooled Permanent-magnet Traction Motor design considering Temporary Overloading. In Proceedings of the 2012 XXth International Conference on Electrical Machines, Marseille, France, 2–5 September 2012; pp. 2677–2682. [CrossRef]
11. Song, K.; Chen, W.; Liu, Y. Design of Oil-Cooled Structure for Switched Reluctance Starter/Generator Based on Multi-Field Coupling. *Electr. Mach. Control. Appl.* **2012**, *39*, 6–11.
12. Di Pietro, C.C.; Lie, S.S.; Elkasabgy, N. Electric Vehicle Motor. U.S. Patent US5682074A, 28 October 1997.
13. Lim, D.H.; Kim, S.C. Thermal Performance of Oil Spray Cooling System for In-Wheel Motor in Electric Vehicles. *Appl. Therm. Eng.* **2014**, *63*, 577–587. [CrossRef]
14. Zhou, P.; Kalayjian, N.R.; Cutler, G.D. Liquid Cooled Rotor Assembly. U.S. Patent US7579725 B2, 25 August 2009.
15. Zysset, E. Liquid Cooled Asynchronous Electric Machine. U.S. Patent US6191511B1, 20 February 2001.
16. Wang, Y. Research on Slot Oil Cooling System for High Torque Density Concentrated Winding Permanent Magnet Motor. Master's Thesis, Harbin Institute of Technology, Harbin, China, 2017. [CrossRef]
17. Swales, S.H.; Turnbull, P.F.; Schulze, B. Oil Cooled Motor/Generator for an Automotive Powertrain. U.S. Patent US8169110 B2, 1 May 2012.
18. Davin, T.; Harmand, S.; Pellé, J.; Yu, R. Experimental Study of Oil Cooling Systems for Electric Motors. *Appl. Therm. Eng.* **2015**, *75*, 1–13. [CrossRef]

19. Wang, Y.; Song, G.; Niu, W. Method for Rapid Calculation of Convective Heat Transfer Coefficient on Surface of Mechanical Components. China Patent CN201610012440.8, 25 May 2016.
20. Zhang, B. Research on Electromagnetic Thermal Design of Permanent Magnet Synchronous Drive Motor for Electric Vehicles. Ph.D. Thesis, Huazhong University of Science and Technology, Wuhan, China, 2015.

Disclaimer/Publisher's Note: The statements, opinions and data contained in all publications are solely those of the individual author(s) and contributor(s) and not of MDPI and/or the editor(s). MDPI and/or the editor(s) disclaim responsibility for any injury to people or property resulting from any ideas, methods, instructions or products referred to in the content.